environmental sciences proceedings

MDPI

Proceeding Paper

Sensitivity Study of Daily Dust Forecast over the Mena Region Using the RegCM4.4 Model †

Zeinab Salah

Egyptian Meteorological Authority, Kobry El Qubba, Cairo P.O. Box 11784, Egypt; zeinabsalah@gmail.com

† Presented at the 6th International Electronic Conference on Atmospheric Sciences, 15–30 October 2023; Available online: https://ecas2023.sciforum.net/.

Abstract: Dust storms are one of the most frequent weather phenomena in the Middle East and North Africa (MENA) region. Therefore, the daily forecast of dust events is vital for different sectors. Many regional models can be used to forecast atmospheric dust storms. Here, the ICTP regional climate model (RegCM4) was used to simulate atmospheric dust emission, transportation, and deposition, using the optical properties of dust particles, over the MENA region. In the current work, the dust optical depth (DOD) obtained using RegCM4 was compared with the aerosol optical depth (AOD) measured by AERONET at different stations and by MODIS. In the first experiment, two datasets (NCEP/GFS and ERA-Interim) for the meteorological initial and boundary conditions have been used, whereas in the second experiment, GFS with two dust emission schemes have been used. In the last experiment, GFS with two values of the erodibility factor (1 and 0.5) have been used. The RegCM4 forecast with GFS and the first dust emission scheme provided higher values of DOD than AERONET. However, when using the reanalysis data of ERA-Interim or the second dust emission scheme, there was no significant difference, but the erodibility factor decreases led to a reduction in the overestimated values.

Keywords: dust; RegCM4; GFS; ERA-Interim; AOD; erodibility factor

check for updates

Citation: Salah, Z. Sensitivity Study of Daily Dust Forecast over the Mena Region Using the RegCM4.4 Model. *Environ. Sci. Proc.* **2023**, *27*, 35. https://doi.org/10.3390/ecas2023-15484

Academic Editor: Anthony Lupo

Published: 30 October 2023

Copyright: © 2023 by the author. Licensee MDPI, Basel, Switzerland. This article is an open access article distributed under the terms and conditions of the Creative Commons Attribution (CC BY) license (https://creativecommons.org/licenses/by/4.0/).

1. Introduction

The MENA region is a critical area for developing a better understanding of the factors involved in the generation of large dust events because it is considered a principal source of atmospheric dust and includes nearly every type of known dust source due to its varied landforms [1,2]. However, data related to the nature of land surfaces in North Africa and to the conditions that lead to the generation of dust storm events are scarce. Numerical models are considered vital tools for forecasting dust storms. Here, the regional climate model version 4, hereinafter, "RegCM4.4" [3], was run with different meteorological initial and boundary conditions with two dust schemes.

This study aimed to improve the daily dust forecast over the MENA region by testing different options in the RegCM4.4 model to determine the optimum conditions. For this purpose, four experiments were performed with different criteria, as illustrated later in the following sections.

2. Data and Methodology

2.1. The Dust Model (RegCM4.4)

RegCM4 is a hydrostatic limited area model for a compressible atmosphere and has been used in various studies of dust emission in various regions of the world. Ref. [4] studied the changes in dust load over some arid regions in India. Ref. [5] used the RegCM4 model to study the impacts of land use change on dust emission in Kuwait, and ref. [6] compared the performance of two dust schemes in RegCM4 for Turkey.

Two dust emission schemes were used in the current study; one (Scheme1) is based on studies by [7–9], and the other (Scheme2) is based on a study by [10].

In RegCM4.4, dust mobilization is parameterized as a function of wind speed exceeding a threshold value, surface roughness, minimum friction velocity [11], and soil moisture [12], while the horizontal mass flux is parameterized in terms of friction velocity, according to [13]. The dust particles are divided into four size bins (0.1–1.0 μm, 1.0–2.5 μm, 2.5–5.0 μm, and 5.0–20 μm). The radiative flux estimation follows the NCAR-CCM3 scheme [14]. Land surface processes are represented by the biosphere–atmosphere transfer scheme "BATS" [15] (Dickinson et al., 1993). The processes in the planetary boundary layer are parameterized using [16], and the cumulus convection processes are described by [17]. The model includes a large-scale, resolvable subgrid explicit moisture scheme (SUBEX) [18].

The studied domain covered North Africa, South Europe, and the Middle East (10° N–60° N, 25° W–60° E), with a resolution of 45 km and 18 vertical sigma levels, with the model top set at 50 hPa. The studied period was from 5 May 2014 to 31 May 2014, and each day, a forecast was made for the next 4 days, but the analysis was conducted using data from the first 24 h of each run.

2.2. Meteorological Data

In this experiment, we used two different sources for the initial and lateral boundary conditions of the atmospheric variables (geopotential height, temperature, relative humidity, and wind). One was the NCEP global forecast system (GFS) with a resolution of 1 degree, and the other consisted of the reanalysis data of ERA-Intrim, with a resolution of 1.5 degrees; the lateral boundary conditions were updated every 6 h.

2.3. AERONET Data

Version 2 Level 1.5 of AERONET products "https://aeronet.gsfc.nasa.gov/ (accessed on 26 August 2023)" was used for the model evaluation over twelve stations, as mentioned in Table 1. The observations were assigned to the nearest hour, and in the case that more than one observation was assigned to the same hour, the average of the measured values was considered. The aerosol optical depth at 550 nm (AOD_{550}) was calculated using AOD at 440, 675, and 870 nm (hereafter AOD_{440}, AOD_{675}, AOD_{870}), and the Ångström exponent 440-870 (AE_440_870) was determined using the Ångström law, as in Equation (1).

$$AOD_{550} = \frac{1}{3}\left[AOD_{440}\left(\frac{440}{550}\right)^{AE_440_870} + AOD_{675}\left(\frac{675}{550}\right)^{AE_440_870} + AOD_{870}\left(\frac{870}{550}\right)^{AE_440_870}\right] \quad (1)$$

Table 1. AERONET stations used in the validation.

Number	Station	Lat	Lon
1	Cairo_EMA_2	30.00	31.00
2	Dakar	14.394	−16.959
3	El_Farafra	27.058	27.990
4	Hada_El-Sham	21.802	39.729
5	IER_Cinzana	13.278	−05.934
6	Ilorin	08.00	04.00
7	Izana	28.309	−16.499
8	Ouarzazate	30.928	−06.913
9	Saada	31.626	−08.156
10	SEDE_BOKER	30.855	34.782
11	Tamanrasset_INM	22.00	05.00
12	Zinder_Airport	13.777	08.990

2.4. MODIS Data

The daily means of combined dark target and deep blue aerosol optical depths at 550 nm for land and ocean, calculated by Terra and Aqua MODIS, with a resolution of 1° × 1°, downloaded from "https://giovanni.gsfc.nasa.gov/giovanni/ (accessed on 26 August 2023)", were used to compare the AOD values with those forecasted by RegCM4.4. The AOD values obtained with Terra and Aqua MODIS were compared with the simulated AOD values at the hours of 9 and 12 UTC, respectively, since these two hours were the nearest times to that of MODIS determinations.

3. Results and Discussion

3.1. Two Different Datasets of the Meteorological Field

Figure 1 shows a comparison of the DOD values resulting from RegCM4.4 using GFS (red line) and ERA-Interim (green line) and AOD at 550 nm calculated through AERONET measurements using Equation (1) (blue dots), in addition to the Ångström exponent at 440–870 nm (purple dots), indicating the particle size (fine or coarse) at the 12 stations listed in Table 1 in the same order.

As shown in Figure 1, the behavior of DOD using GFS and ERA-Interim was not consistent in most cases in the selected stations; however, approximately the same behavior was found at the station of IER_Cinzana during the period of 14–20 May 2014, with different values of DOD; with GFS, DOD exceeded 2, but with ERA-Interim its value was less than 0.5, which was more consistent with the AOD obtained with AERONET. At the station of Izana, DOD resulting from ERA-Interim was near the measured AOD value, whereas at the stations of Cairo_EMA_2, Dakar, El_Farafra, Hada_El-Sham, Saada, and SEDE_BOKER, RegCM4.4 with GFS provided DOD values near the observed ones. Moreover, at Zinder_Airport station, RegCM4.4 using GFS captured high values of DOD on 9 and 21 May 2014, which agreed with the AERONET data and the measured Ångström exponent (AE) (AE_440-870 < 0.5), indicating that the high values of AOD corresponded to dust events. In contrast, RegCM4.4 with ERA resulted in lower values of DOD.

3.2. Two Different Dust Emission Schemes

In this experiment, RegCM4.4 was run using GFS data from two dust emission schemes. Figure 2 shows the DOD values produced by RegCM4.4 using scheme1 (red line) and scheme2 (green line), the AERONET AOD at 550 nm (blue dots), and the Ångström exponent at 440–870 nm (purple dots). One can notice that the two schemes resulted in the same behavior at all stations but with different values of dust optical depth, as in the stations of Cairo_EMA_2 and El_Farafra on 29 and 31 May 2014, when DOD with scheme1 exceeded 1, whereas DOD with scheme2 was more consistent with AOD from AERONET. In the station of IER_Cinzana, the two schemes resulted in more dust causing high values of DOD exceeding 1.5 in the period of 15–19 May 2014, whereas the AERONET AOD values were $\leq$0.5. Moreover, the same was observed at the station of Izana on 10–22 May 2014 and at the station of Zinder_Airport on 12–19 May 2014.

3.3. Two Values for the Dust Emission Adjustment Factor

The dust flux is directly proportional to the fraction of erodible surface (E), which is related to the fraction of the uncovered surface according to the presence of roughness elements and the exposure to wind erosion. Ref. [19] showed that the fraction of erodible surface roughly decreases as a function of the roughness length (Z0) in desert regions. When Z0 is less than 3×10^{-3} cm, the desert surface can be considered as totally erodible (E = 1), whereas when Z0 exceeds 3×10^{-3} cm, E can be calculated as a linear function of the logarithm of Z0 according to the equation of [20]:

$$E = 0.7304 - (0.0804 \times \log_{10}(Z0)) \quad (2)$$

In this experiment, the RegCM4.4 model was run using GFS data and scheme1, but with two values of the dust emission adjustment factor (or soil erodibility), i.e., 1 and 0.5. Figure 3 shows the DOD values obtained with RegCM4.4 assuming the adjustment factor equaled 1 and 0.5, represented in red and green lines, respectively, the AERONET AOD at 550 nm (blue dots), and the Ångström exponent at 440–870 nm (purple dots).

From the previous experiments, one can notice the high values of AOD that exceeded 2 in some cases, in contrast with those provided by AERONET. Therefore, these values could cause a false alarm, forecasting the arrival of a severe dust storm.

The changes in the erodibility factor had an effective influence on the DOD values. Using the erodibility factor of 0.5 resulted in a noticeable decrease in DOD at the stations of Cairo_EMA_2 and El-Farafra in the last days of May, in addition to the stations of IER_Cinzana, Izana, Ouarzazate, and Zinder_Airport in the middle of May.

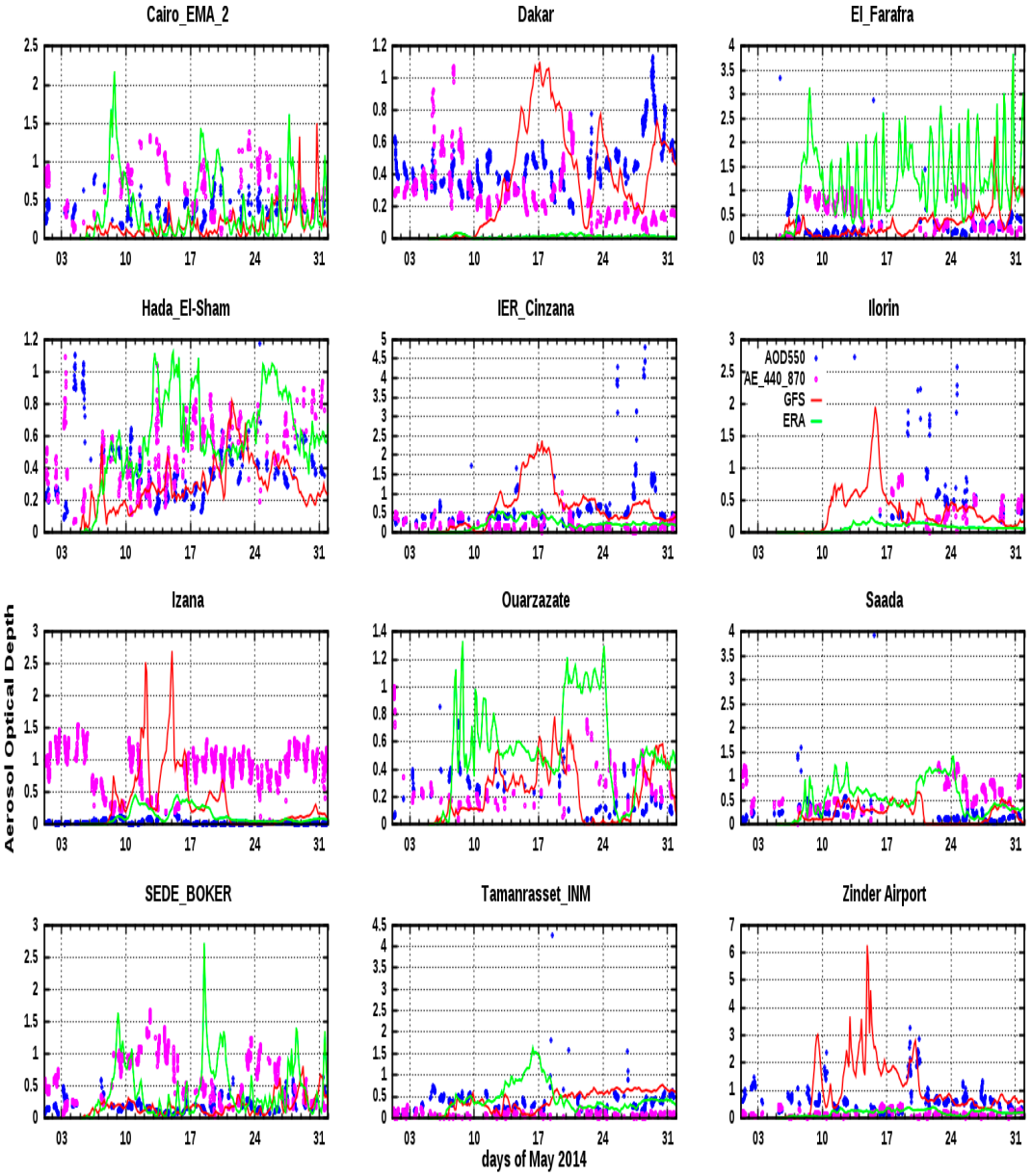


Figure 1. The daily variations in AOD in the visible band during May 2014, simulated by RegCM4 with different initial meteorological fields (red line refers to GFS, and green line refers to ERA-Interim), compared with AOD at 550 nm calculated by AERONET (blue dots) and AE at 440–870 nm (pink dots), over some stations. The stations are in the same order as in Table 1.

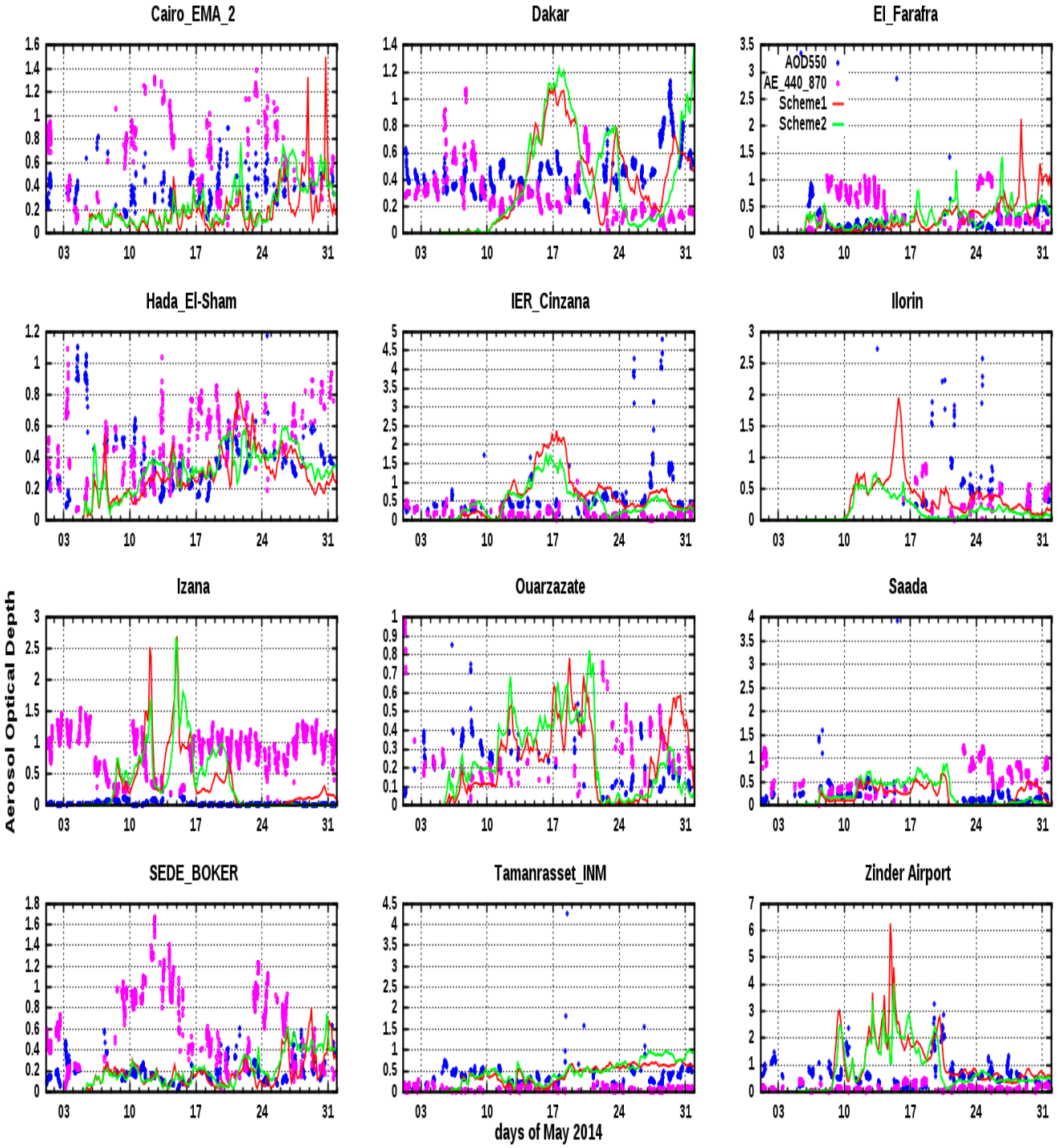


Figure 2. The daily variations in AOD in the visible band during May 2014, simulated by RegCM4 with different emission schemes (red line refers to Scheme1, and green line refers to Scheme2), compared with AOD at 550 nm calculated with AERONET (blue dots) and AE at 440–870 nm (pink dots), at some stations. The stations are in the same order as in Table 1.

3.4. Comparison with MODIS/Aqua Measurements

The average AOD values in the whole studied period were calculated using Terra and Aqua MODIS, and then the difference between DOD values obtained with RegCM4.4 at 9 and 12 UTC and the calculated average AOD values of Terra and Aqua MODIS, respectively, was calculated, as shown in Figures 4 and 5, respectively. It can be noticed that AOD values resulting from the GFS_1_0.5 experiment (GFS data and scheme1 with

erodibility factor = 0.5) for Sahara have low bias compared with those obtained in the other experiments.

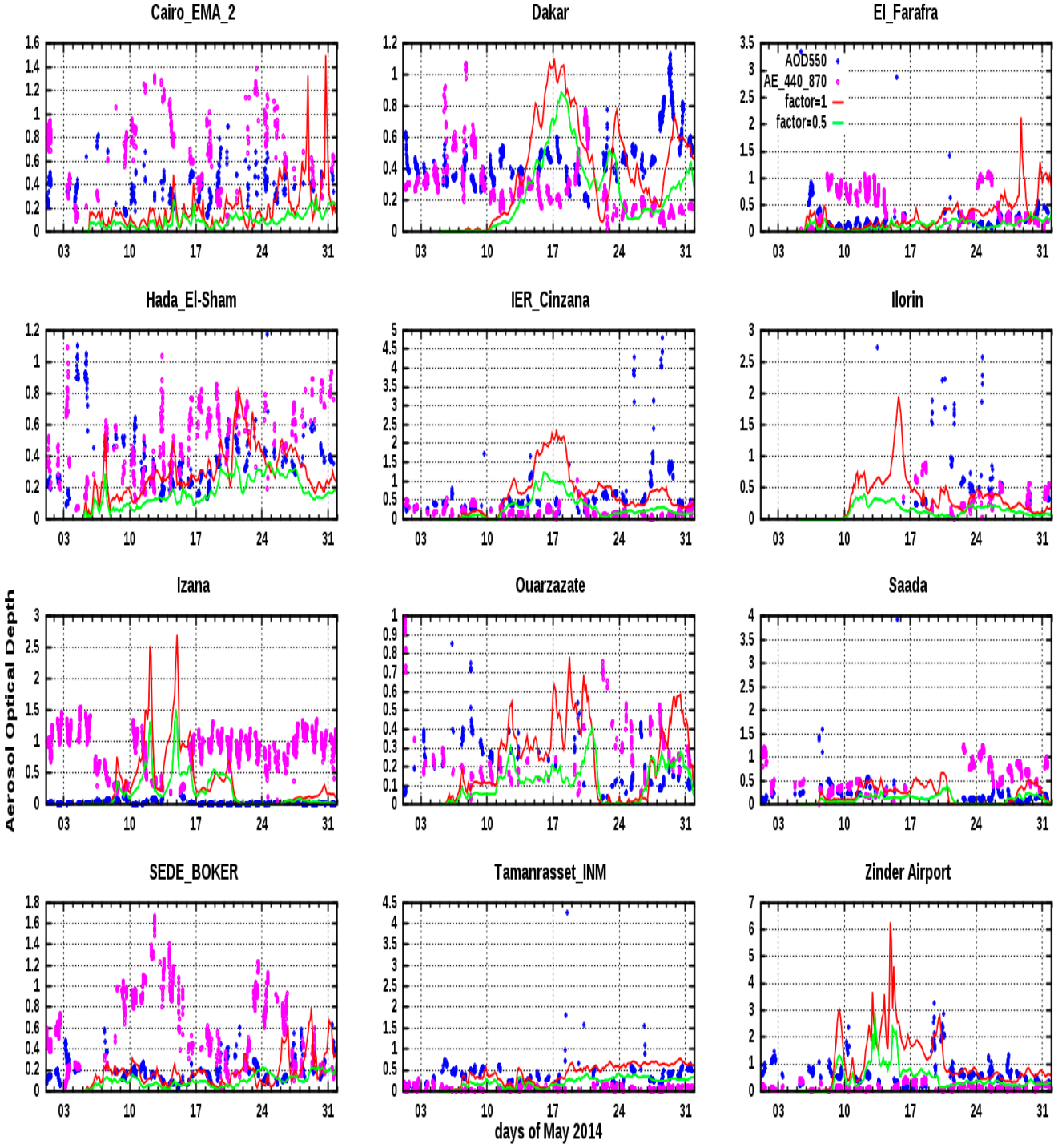


Figure 3. The daily variations in AOD in the visible band during May 2014, simulated by RegCM4 with different values of erodibility factor (red line refers to the value of 1, and green line refers to the value of 0.5), compared with AOD at 550 nm calculated with AERONET (blue dots) and AE at 440–870 nm (pink dots), at some stations. The stations are in the same order as in Table 1.

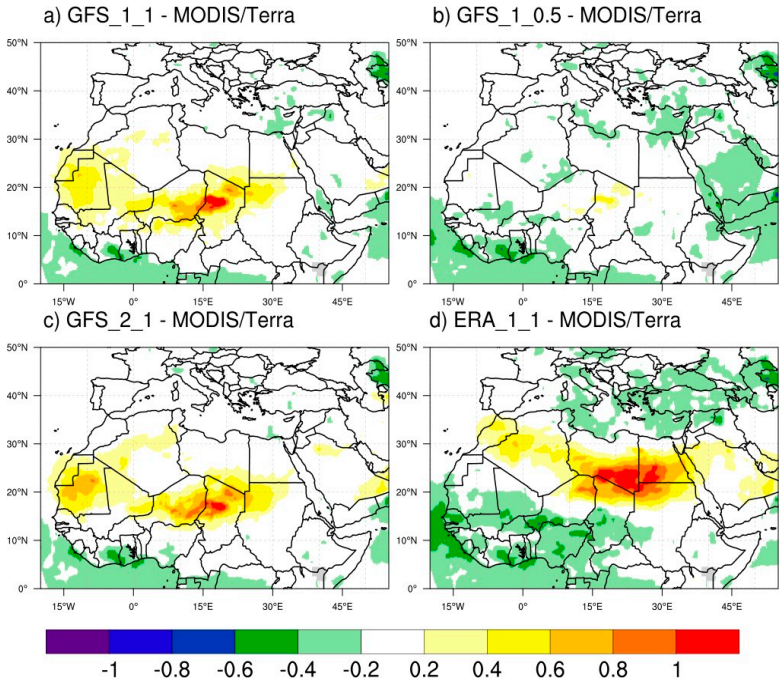


Figure 4. The differences between the average DOD values calculated over the whole studied period simulated in four different experiments: (**a**) GFS_1_1 (GFS and scheme1 with erodibility factor = 1), (**b**) GFS_1_0.5 (GFS and scheme1 with erodibility factor = 0.5), (**c**) GFS_2_1 (GFS and scheme2 with erodibility factor = 1), (**d**) ERA_1_1 (ERA−Interim and scheme1 with erodibility factor = 0.5), compared to AOD values from Terra.

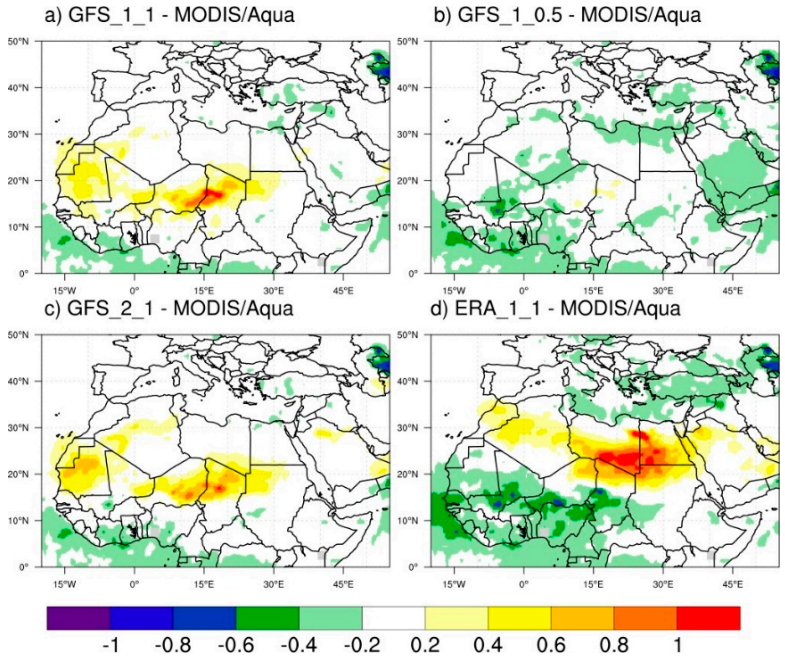


Figure 5. The differences between the average DOD values calculated over the whole studied period simulated in four different experiments: (**a**) GFS_1_1 (GFS and scheme1 with erodibility factor = 1), (**b**) GFS_1_0.5 (GFS and scheme1 with erodibility factor = 0.5), (**c**) GFS_2_1 (GFS and scheme2 with erodibility factor = 1), (**d**) ERA_1_1 (ERA−Interim and scheme1 with erodibility factor = 0.5), compared to AOD values from Aqua.

4. Conclusions

In this study, different options were chosen to run the RegCM4.4 model to forecast dust emissions over the MENA region. These options included: (1) data from two meteorological fields, i.e., the NCEP-GFS forecast and the ERA-Interim reanalysis, (2) two different dust emission schemes, (3) two values of the soil erodibility factor. These experiments were limited to only one month of daily dust forecast.

The high values of dust optical depth that were obtained posed the most noticeable problem in our forecast. Therefore, by testing different options, we found that changing the erodibility factor value, while using the first dust scheme, caused a significant reduction in AOD at some AERONET stations. Also, the two dust emission schemes resulted in the same behavior at all stations but with different values of dust optical depth.

Finally, it is necessary to perform more experiments using different planetary boundary layer schemes, land surface models, convection schemes, and the radiation schemes available in RegCM4.4 over a long period to improve the forecast of dust emissions using RegCM4.4.

Funding: This research received no external funding.

Data Availability Statement: Data are available in this manuscript, in the mentioned websites.

Acknowledgments: The author thanks the principal investigators and their staff for establishing and maintaining the AERONET sites considered in this investigation. Public access to the Global Forecast System (GFS) forecast meteorological data provided by the National Center for Environmental Prediction (NCEP) and the ERA Interim Reanalysis dataset provided by the European Center for Medium-Range Weather Forecasts (ECMWF) is gratefully acknowledged.

Conflicts of Interest: The author declares no conflicts of interest.

References

1. Middleton, N.J.; Goudie, A.S. Saharan dust: Sources and trajectories. *Trans. Inst. Br. Geogr.* **2001**, *26*, 165–181. [CrossRef]
2. Prospero, J.M.; Ginoux, P.; Torres, O.; Nicholson, S.E.; Gill, T.E. Environmental characterization of global sources of atmospheric soil dust identified with the Nimbus 7 Total Ozone Mapping Spectrometer (TOMS) absorbing aerosol product. *Rev. Geophys.* **2002**, *40*, 1002. [CrossRef]
3. Giorgi, F.; Coppola, E.; Solmon, F.; Mariotti, L.; Sylla, B.M.; Bi, X.Q. RegCM4: Model description and illustrative basic performance over selected CORDEX domains. *Clim. Res.* **2011**, *52*, 7–29. [CrossRef]
4. Asutosh, A.; Pandey, S.K.; Vinoj, V.; Ramisetty, R.; Mittal, N. Assessment of Recent Changes in Dust over South Asia Using RegCM4 Regional Climate Model. *Remote Sens.* **2021**, *13*, 4309. [CrossRef]
5. Salah, Z.; Dashti, H.; Zakey, A.; Abdel Wahab, M.M. How land use change can improve air quality status over Kuwait. *Int. J. Environ. Sci. Technol.* **2022**, *19*, 747–762. [CrossRef]
6. Kuzu, S.L.; Yavuz, E. Comparison of RegCM dust schemes by monitoring an aeolian dust transport episode. *Air Qual. Atmos. Health* **2021**, *14*, 2047–2057. [CrossRef]
7. Alfaro, S.C.; Gomes, L. Modeling mineral aerosol production by wind erosion: Emission intensities and aerosol size distribution in source areas. *J. Geophys. Res.* **2001**, *106*, 18075–18084. [CrossRef]
8. Shao, Y. A model for mineral dust emission. *J. Geophys. Res.* **2001**, *106*, 20239–20254. [CrossRef]
9. Zakey, A.S.; Solmon, F.; Giorgi, F. Implementation and testing of a desert dust module in a regional climate model. *Atmos. Chem. Phys.* **2006**, *6*, 4687–4704. [CrossRef]
10. Kok, J.F. A scaling theory for the size distribution of emitted dust aerosols suggests climate models underestimate the size of the global dust cycle. *Proc. Natl. Acad. Sci. USA* **2011**, *108*, 1016–1021. [CrossRef] [PubMed]
11. Marticorena, B.; Bergametti, G. Modeling the atmospheric dust cycle: 1. Design of a soil derived dust production scheme. *J. Geophys. Res.* **1995**, *100*, 16415–16430. [CrossRef]
12. Fécan, F.; Marticorena, B.; Bergametti, G. Parameterization of the increase of the aeolian erosion threshold wind friction velocity due to soil moisture for arid and semi-arid areas. *Ann. Geophys.* **1999**, *17*, 149–157. [CrossRef]
13. Sun, H.; Pan, Z.; Liu, X. Numerical simulation of spatial–temporal distribution of dust aerosol and its direct radiative effects on East Asian climate. *J. Geophys. Res.* **2012**, *117*, 1–14. [CrossRef]
14. Kiehl, J.T.; Hack, J.J.; Bonan, G.B.; Boville, B.A.; Briegleb, B.P.; Williamson, D.L.; Rasch, P.J. *Description of the NCAR Community Climate Model (CCM3). (No. NCAR/TN-420+STR)*; University Corporation for Atmospheric Research: Boulder, CO, USA, 1996. [CrossRef]

15. Dickinson, R.E.; Henderson-Sellers, A.; Kennedy, P.J. *Biosphere-Atmosphere Transfer Scheme (BATS) Version 1e as Coupled to the NCAR Community Climate Model (No. NCAR/TN-387+STR)*; University Corporation for Atmospheric Research: Boulder, CO, USA, 1993. [CrossRef]
16. Holtslag, A.; de Bruijn, E.; Pan, H.L. A high resolution air mass transformation model for short range weather forecasting. *Mon. Weather Rev.* **1990**, *118*, 1561–1575. [CrossRef]
17. Emanuel, K. A scheme for representing cumulus convection in large scale models. *J. Atmos. Sci.* **1991**, *48*, 2313–2335. [CrossRef]
18. Pal, J.S.; Small, E.E.; Eltahir, E.A.B. Simulation of regional-scale water and energy budgets: Representation of subgrid cloud and precipitation processes within RegCM. *J. Geophys. Res. Atmos.* **2000**, *105*, 29579–29594. [CrossRef]
19. Laurent, B.; Marticorena, B.; Bergametti, G.; Mei, F. Modeling mineral dust emissions from Chinese and Mongolian deserts. *Glob. Planet. Chang.* **2006**, *52*, 121–141. [CrossRef]
20. Laurent, B.; Marticorena, B.; Bergametti, G.; Léon, J.F.; Mahowald, N.M. Modeling mineral dust emissions from the Sahara Desert using new surface properties and soil database. *J. Geophys. Res.* **2008**, *113*, D14218. [CrossRef]

Disclaimer/Publisher's Note: The statements, opinions and data contained in all publications are solely those of the individual author(s) and contributor(s) and not of MDPI and/or the editor(s). MDPI and/or the editor(s) disclaim responsibility for any injury to people or property resulting from any ideas, methods, instructions or products referred to in the content.